A&A 652, A113 (2021)
https://doi.org/10.1051/0004-6361/202141391

Astronomy & Astrophysics

The Venus Express observation of Venus' induced magnetosphere boundary at solar maximum

Q. Xu (徐麒)[1,2], X. Xu (徐晓军)[1,2], T. L. Zhang (张铁龙)[3,4], Z. J. Rong (戎昭金)[5,6], M. Wang (王明)[1,7,2], J. Wang (王晶)[8,2], Y. Ye (叶煜东)[1,2], Z. Zhou (周梓露)[1,2], Q. Chang (常清)[1,2], J. Xu (徐佳莹)[1,2], X. Wang (王星)[1,2], and L. Luo (罗磊)[1,2]

[1] State Key Laboratory of Lunar and Planetary Sciences, Macau University of Science and Technology, Macau, PR China
e-mail: xjxu@must.edu.mo
[2] CNSA Macau Center for Space Exploration and Science, Macau, PR China
[3] Harbin Institute of Technology, Shenzhen, PR China
[4] Space Research Institute, Austrian Academy of Sciences, Graz, Austria
[5] Key Laboratory of Earth and Planetary Physics, Institute of Geology and Geophysics, Chinese Academy of Sciences, Beijing, PR China
[6] College of Earth and Planetary Sciences, University of Chinese Academy of Sciences, Beijing, PR China
[7] Institute of Space Weather, Nanjing University of Information Science and Technology, Nanjing, PR China
[8] Planetary Environmental and Astrobiological Research Laboratory (PEARL), School of Atmospheric Sciences, Sun Yat-sen University, Zhuhai, Guangdong, PR China

Received 26 May 2021 / Accepted 28 June 2021

ABSTRACT

The Venusian plasma environment is divided into two distinct regions by the induced magnetosphere boundary (IMB): the domain of solar wind protons and the domain of local planetary ions. Previous studies on the identification of the IMB gave various IMB definitions. Here we study the well-structured Venusian IMB with a sudden magnetic field rotation and a sharp magnetosheath plasma decrease using Venus Express observations. We statistically investigate the location of such well-structured IMB and give an average location of the IMB at solar maximum. The solar activity and solar wind controls of the Venusian IMB location is also studied in this work. Our results show that the dayside Venusian IMB distance increases with solar activity, but it decreases with increasing solar wind dynamic pressure and interplanetary magnetic field cone angle. The behaviors of the IMB under these conditions are similar to those of the ionopause, indicating that the distance of the Venusian IMB is much correlated with the scale of the ionosphere. We suggest that the variation of the IMB is partially contributed to by the variation of the ionopause, whose altitude is determined by the pressure balance between ionospheric thermal pressure and external magnetic pressure.

Key words. planets and satellites: individual: Venus – interplanetary medium – planets and satellites: magnetic fields

1. Introduction

The direct interaction of solar wind with Venus' ionosphere produces an induced magnetosphere around the planet (Luhmann et al. 2004). The induced magnetosphere is a region where the magnetosheath plasma flow with a frozen magnetic field is strongly mass-loaded by planetary particles and the magnetic flux piles up. The induced magnetosphere is separated from the inner magnetosheath by an upper boundary named the induced magnetosphere boundary (IMB). The IMB is a narrow layer with a strong current system with a local ion gyroradius or inertial length (Bertucci et al. 2011). The solar wind is compressed and heated when crossing the bow shock into the magnetosheath (Phillips & McComas 1991; Bertucci et al. 2011). At the IMB, the solar wind ions are decelerated by the Lorentz force (Dubinin et al. 2011). In the induced magnetosphere, the measured plasma temperature decreases (Spenner et al. 1980). Though the IMB is not an impenetrable boundary, most solar wind is shielded at the IMB (Zhang et al. 1991, 2007). The IMB is usually a magnetic discontinuity (Saunders & Russell 1986; Bertucci et al. 2005; Zhang et al. 2008b) similar to the Earth's magnetopause. The interplanetary magnetic field (IMF) lines anchored by planetary plasma in the induced magnetosphere, to some extent, can be treated as a part of the planet.

The transition layer from the magnetosheath to the induced magnetosphere at Venus was previously called the ionosheath boundary (ISB, Spenner et al. 1980), the upper boundary of the magnetic barrier (Zhang et al. 1991), the magnetic pileup boundary (MPB, Bertucci et al. 2003), the induced magnetopause (Zhang et al. 2007), the ion composition boundary (ICB, Martinecz et al. 2008), the upper mantle boundary (UMB, Martinecz et al. 2009), and the induced magnetosphere boundary (IMB, Barabash et al. 2007b). Bertucci et al. (2011) suggested all of these names can be grouped together and referred to as the IMB because they do not contradict each other. However, the characteristics of the Venusian IMB are still ambiguous based on previous observations. From the bow shock to the ionopause, a sharp jump in the magnetic field strength representing the IMB is observed in part of the PVO OMAG data (Bertucci et al. 2003). However, the increase in the magnetic field strength is usually gradual in the inner magnetosheath of Venus (Zhang et al. 1991, 2008b). Bertucci et al. (2003) identified the IMB characterized by the enhancement of magnetic

field draping, even though the magnetic field is smooth. Using only the magnetic field data from Venus Express (VEX), Zhang et al. (2008a) identified the IMB at the place where the magnetosheath waves stop. The cessation of magnetic field oscillation and the change of field direction are observed simultaneously at the IMB, indicating a directional discontinuity of the magnetic field (Zhang et al. 2008b). However, these two features do not always take place in every orbit of VEX. The plasma properties at the IMB have been discussed since Venera-9 and Venera-10 missions. Vaisberg et al. (1976) observed the decrease in the plasma energy and temperature at the boundary layer of the magnetotail, which suggested the ion composition changes from solar wind into planetary-origin ions at the IMB. Then the PVO mission verified the cooling of electrons at the IMB (Spenner et al. 1980). Martinecz et al. (2008) reported the existence of an ion composition boundary through VEX ASPERA-4 observation. A definite criterion, which is the sharp decrease in electron fluxes with energies greater than 35 eV, was proposed to identify the IMB (Martinecz et al. 2009).

Solar activities control the location of Venusian IMB (Zhang et al. 1990, 2008a). The higher altitude of IMB, as well as the ionopause and bow shock, at solar maximum is attributed to the higher solar extreme ultra-violet (EUV) radiation (Russell et al. 1988; Zhang et al. 2008a; Han et al. 2020). The increased EUV flux leads to a larger obstacle indicated by the expanded ionosphere and exosphere (Fox & Sung 2001). The elevated ionopause at solar maximum would raise the upper boundary IMB. The effect of solar wind on Venusian IMB is less discussed in previous studies. Zhang et al. (1991) investigated the dependence of the IMB on the solar wind dynamic pressure and found that the altitude of IMB decreases with increasing dynamic pressure. The magnetic pressure at the IMB also increases when the dynamic pressure becomes higher (Ma et al. 2020). As for some extreme solar wind conditions, variations in the IMB would be more complicated (Collinson et al. 2015; Xu et al. 2019). The increase in the magnitude and cone angle of the IMF (the latter being the angle between solar wind velocity and the IMF direction) leads to a stronger induced magnetosphere (Chang et al. 2018; Xiao & Zhang 2018), but the variation in the IMB location has yet to be investigated.

Previous observations of the Venusian IMB have only been based on magnetic field data or plasma measurements (Zhang et al. 1991, 2008a; Martinecz et al. 2009). The gradual change in the magnetic field at the IMB is inconsistent with the definition of a "thin" and "sharp" boundary which is proposed by Bertucci et al. (2011). The change in ion compositions might be a good indicator dividing the two regions, but the low-resolution ion mass and moment data only give a rough estimation of the IMB position (Barabash et al. 2007b; Fedorov et al. 2011). The strong decrease in electron flux determines a sharp boundary (Martinecz et al. 2009), but sometimes it is a gradual decrease. These definitions and descriptions of the IMB are incomplete. VEX's entire mission almost covered the whole Solar Cycle 24. The induced magnetosphere usually sinks into the ionosphere at solar minimum for the weak ionospheric thermal pressure controlled by the low solar irradiance, leading to some coincidence of the IMB and ionopause (Zhang et al. 2008a). At solar maximum, VEX's observations demonstrate well-defined regions and boundaries for solar wind-Venus interactions. The average IMB location has been estimated at solar minimum (Zhang et al. 2008a; Martinecz et al. 2009), but not yet at solar maximum based on VEX data. Since Solar Cycle 24 is extremely weak (Chang et al. 2018), the Venusian IMB might be depressed compared with previous solar cycles. In this work, we attempt to identify the well-structured Venusian IMB with both magnetic field and plasma criteria based on VEX's measurements. The average position of the IMB at solar maximum is determined. Furthermore, we study the effects of solar wind and the IMF on the IMB position.

2. Instrument and data

Venus Express carried out an elliptic polar orbit with a period of 24 h (Svedhem et al. 2007). The induced magnetosphere in terminator is covered for the obiter periapsis located at about 80° north latitude with an altitude of ~250 km. The apoapsis of ~66 000 km ensures that the upstream solar wind condition could be measured for every orbit. The Analyzer of Space Plasmas and Energetic Atoms (ASPERA-4; Barabash et al. 2007a) contains the ion mass analyzer (IMA) and the electron spectrometer (ELS), providing ion fluxes (12-s resolution) in the energy range of 0.01–30 keV q^{-1} and electron fluxes (4-s resolution) in that of 0.01–20 keV q^{-1}. The IMA conducts a full 3D scan to generate the 192-s resolution data of plasma density and velocity (Fedorov et al. 2011). The magnetometer (MAG) instrument (Zhang et al. 2006) measures the magnetic field with a time resolution of 1 s. The plasma spectra and magnetic field data are used for IMB identification, while the 192-s resolution moment data of a proton from Fedorov et al. (2011) are used to determine the solar wind condition. This work uses the Venus Solar Orbital (VSO) coordinates, in which the X-axis points from Venus to the Sun, the Y-axis is opposite to Venus' orbital velocity, and the Z-axis is northward.

3. Observations

3.1. The characteristics of the Venusian IMB

Since the solar wind is deflected at the IMB, the decrease or disappearance of sheath particles is the principle to identify the IMB. The complete criteria of IMB features were proposed by Bertucci et al. (2011). Limited by VEX measurements, some of the features, such as the decrease in the electron temperature and solar wind density, are not included in our identification criteria. Furthermore, the feature of enhanced magnetic field draping as defined in Bertucci et al. (2003) is excluded considering the complicated data processing. The Venusian IMBs are identified by observing the following changes: (a) a sharp increase in the magnetic field strength (Bertucci et al. 2003); (b) a decrease in the magnetic field fluctuations (Zhang et al. 2008a); (c) an increase in the B_X component and the rotation of the magnetic field orientation (Bertucci et al. 2003; Zhang et al. 2008b); (d) a strong decrease in the electron (E > 35 eV) counts (Martinecz et al. 2009); and (e) a strong decrease in the ion (1 keV) counts considering the effect on shielding the solar wind. We note that not all of these signatures can be observed in one orbit and not every criterion decides the same IMB position. We present two cases exhibiting the behaviors at such well-structured IMB.

Figure 1a shows the magnetic field and plasma observations around the Venusian-induced magnetosphere on 29 July 2011. Panels in Fig. 1a display the magnetic magnitudes ($|B|$), the three magnetic field components, the ion spectrum, the electron spectrum, the altitude and the solar zenith angle (SZA), respectively. The same observations for the day after are shown in Fig. 1b. The magnetosheath is bounded by the IMB and bow shock, which are marked by the vertical lines. Compared with the upstream solar wind, the magnetic field is turbulent and the plasma is heated in the magnetosheath, but the fluctuations in the magnetic field

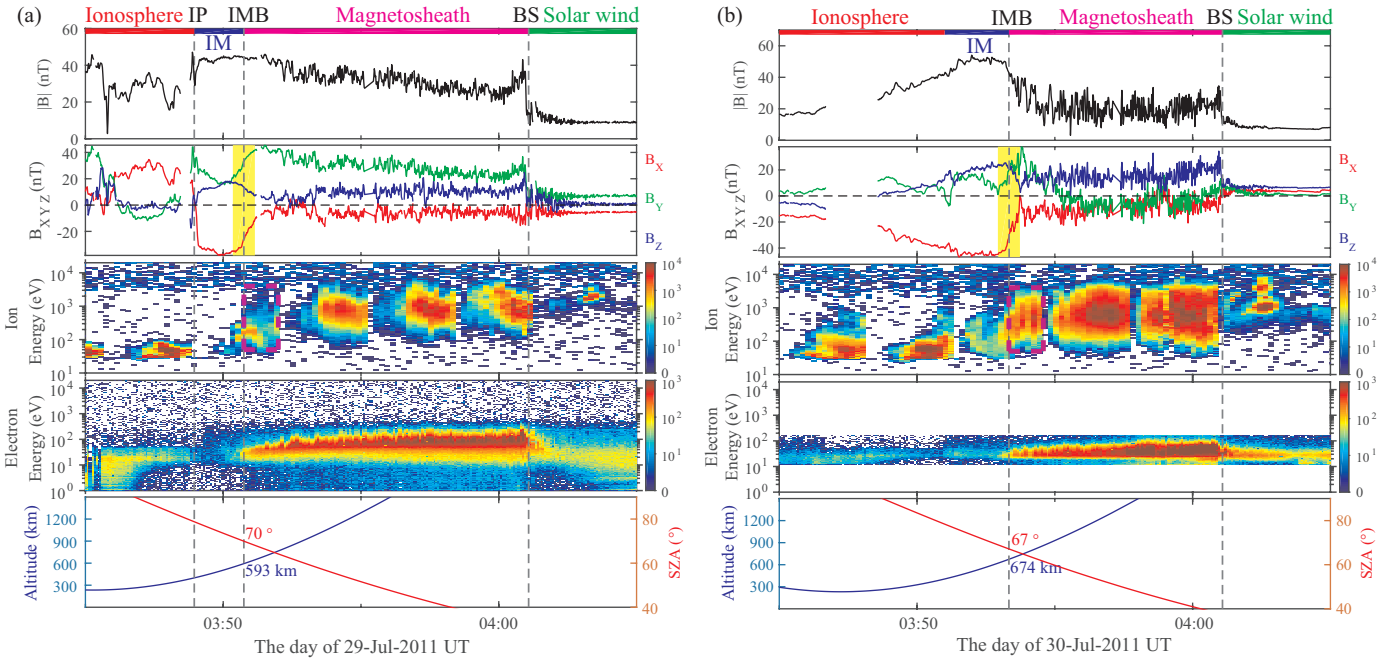

Fig. 1. Identification of the Venusian-induced magnetosphere. *From top to the bottom*, the panels show the magnetic magnitude ($|B|$), the three magnetic field components (B_X, B_Y, B_Z) in VSO coordinates, the ion energy spectra, the electron energy spectra, the altitude, and the solar zenith angle (SZA). The vertical dashed lines mark the ionopause (IP), the induced magnetosphere boundary (IMB), and the bow shock (BS). The induced magnetosphere (IM) is bounded by the ionopause and the IMB. The yellow-shaded boxes mark the rotation of the magnetic field. The altitude and SZA of the IMB are labeled.

decrease when approaching the IMB. Meanwhile, the dissipation of high energy ions and electrons proceeds gradually in the inner magnetosheath as labeled by the dashed rectangles. When arriving at the IMB, the magnetosheath ion counts decrease suddenly and the low-energy ion population appears to be predominant in the induced magnetosphere. The change in the plasma population at the IMB is accompanied by a magnetohydrodynamics (MHD) discontinuity (Bertucci et al. 2005; Zhang et al. 2008b) characterized by an enhancement in the magnetic field strength and/or a rotation of the magnetic field direction as marked by the yellow boxes. The increase in the B_X component at the IMB indicates the enhancement of magnetic field draping at a high SZA region. The field strength $|B|$ increases sharply when encountering the IMB in Fig. 1b, while Fig. 1a reveals another situation of gradual increase in $|B|$. It is noted that the sharp increase in the magnetic field strength at the IMB is observed in only one-fourth of the data. The drop in the plasma flux and the changes in the magnetic field are both observed at the IMB. The ionopause defined by the appearance of photoelectrons (Coates et al. 2008; Cui et al. 2011) is also labeled here. Both the magnetic field strength and direction change at the ionopause where strong diamagnetic currents exist. The region bounded by the IMB and ionopause is the induced magnetosphere (Bertucci et al. 2011).

The sharp increase in $|B|$ could be theoretically predicted (Dubinin et al. 2006) and observed (Bertucci et al. 2003) as a main feature. Such a sharp $|B|$ increase defines a boundary layer with a strong magnetic pressure gradient force which stops the intruding solar wind, but the $|B|$ exhibits a very gradual increase at the Venusian IMB for most crossings. This result is also evident by PVO observations (Zhang et al. 1991; Bertucci et al. 2003). Basically, the induced magnetosphere is a plasma region where the planetary-origin particles dominate (Bertucci et al. 2011). The main population is altered to planetary ions at the IMB and the IMF is mass-loaded by the local heavy ions inside the induced magnetosphere. From the ion spectra in Fig. 1, we could see the drop in magnetosheath ion flux (around 1 keV) at the IMB. In fact, the ion flux starts to decrease gradually in the inner magnetosheath as shown by the dashed rectangles. Correspondingly, the magnetic field oscillation is weakened in the inner magnetosheath. This region displays characteristics similar to the plasma depletion region (PDR) at Earth and Mars (Øieroset et al. 2004; Wang et al. 2020). The depletion of the solar wind plasma is not confined to the IMB, but also in a broader region of the magnetosheath. As for the case in Fig. 1a, the population of strongly reduced hot magnetosheath protons after crossing the PDR-like region contributes little to the total pressure. The higher ion flux marked by a rectangle in Fig. 1b indicates that the plasma depletion concentrates at the IMB because the PDR-like region might be narrow or less effective. Therefore, the increase (decrease) in $|B|$ (plasma flux) from the magnetosheath to the induced magnetosphere can be either smooth or abrupt. Nevertheless, the IMB can still be well identified by the rotation of the magnetic field and the exclusion of the solar wind particles.

3.2. The average IMB location at solar maximum

From July 2011 to November 2014, the magnetic field data and plasma data near the IMB were simultaneously recorded in 556 orbits. Apart from the gradual change in the magnetic field, the plasma signatures may also be absent for the discontinuous ion spectra and sometimes electron spectra with smooth fluxes. The well-structured IMB with both a sudden magnetic field direction change and a sharp plasma flux decrease are selected manually. For our statistical study, 361 well-structured dayside IMB crossings covering the SZA from 45° to 90° are used. Constrained by the orbital geometry of VEX (Barabash et al. 2007a), the IMB in subsolar region is not observed. In Fig. 2, we use the

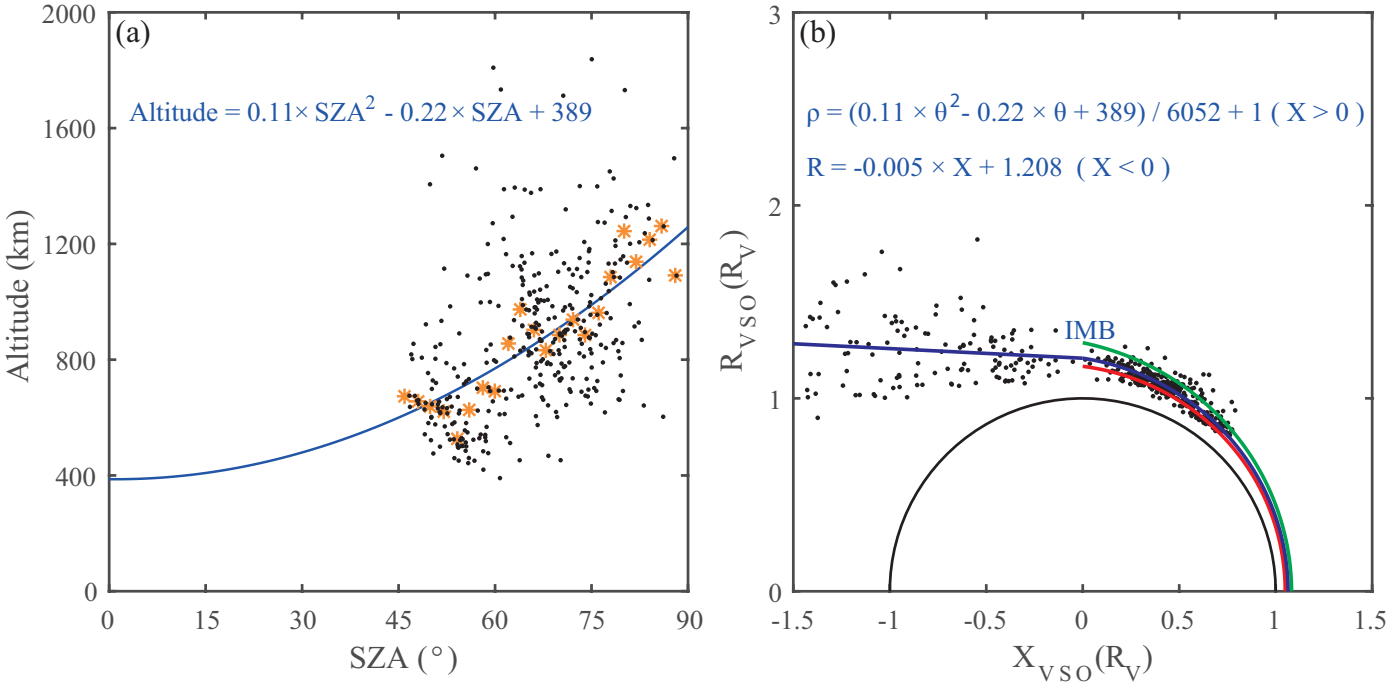

Fig. 2. Average position of the Venusian IMB at solar maximum. (*a*) The altitude of the dayside IMB (marked by black dots) as a function of SZA. The orange asterisks are the median value of these altitudes. The blue curve is the fitted altitude based on the median altitudes. (*b*) The IMB crossings (black dots), the fitted IMB location (blue line), the IMB location at solar minimum from Zhang et al. (2008a) (red line), and the IMB location at solar maximum from Zhang et al. (1991) (green line). The nightside IMB distance R_{VSO} is fitted as a function of X_{VSO}.

second-order polynomial curve (Zhang et al. 1991, 2008a) to fit the median altitudes of the dayside IMBs at different SZAs:

$$\text{Altitude(SZA)} = 0.11 \times \text{SZA}^2 - 0.22 \times \text{SZA} + 389 \quad (0^\circ \le \text{SZA} \le 90^\circ) \tag{1}$$

The IMB with field rotation is rarely observed on the nightside. The nightside IMB, or the magnetotail boundary (Rong et al. 2014), is identified only based on the drop in the plasma flux. The linear fit was used to estimate the average position on the nightside:

$$R = -0.005 \times X + 1.208 \ (X < 0). \tag{2}$$

The fit result is not good because the distributions of nightside IMB crossings are very scattered, as presented in Fig. 2b. Therefore the linear fit of the nightside IMB is only used for estimating the average flaring angle (Angsmann et al. 2011), but not for the following statistical study. The average flaring angle is almost parallel to the X-axis (Fedorov et al. 2008).

The estimated IMB altitude at solar maximum is 387 km at subsolar point (SZA = 0°) and 1258 km at the terminator (SZA = 90°). These locations are higher than those at solar minimum (Zhang et al. 2008a), but lower than those observed by the PVO at solar maximum (Zhang et al. 1991). The IMB altitude is closely related to solar cycles. The solar activity is very weak in Solar Cycle 24 compared with previous cycles when the PVO was operational (Chang et al. 2018). The daily average sunspot number (SSN) for the 361 cases was calculated to be 67. The comparison of IMB locations during different solar phases is summarized in Table 1 and Fig. 2b. As the solar activity decreases, the IMB gets closer to the planet. It seems that the IMB altitude at the terminator is approximately linearly dependent on the SSN. The IMF magnitude is also dependent on solar activity (Chang et al. 2018). The dependence of the IMB location on the IMF magnitude is still not clear.

3.3. The effects of solar wind and IMF on the IMB

The average IMB altitude is controlled by the solar activity, as discussed above. However, during a specific solar phase, the solar wind condition might also be significant in influencing the IMB altitude. To investigate the dependence of the Venusian IMB location on the solar wind dynamic pressure, the solar wind velocity, the IMF magnitude, and the IMF orientation, the linear regression was carried out to analyze the effect of each of these variants. The reliability of the regression result was decided by the *P*-value of the *F* test, where the significance level was set to 0.01 (Chai et al. 2014). The nightside IMB was not included in these statistics because the scattered nightside data points in Fig. 2b are not appropriate for linear regression analysis. For each dayside IMB crossing, the average value of 15 min of data upstream from the bow shock was adopted as the upstream solar wind and IMF conditions. The thin foreshock region was not excluded in the 15 min. To compare the IMB altitude of various orbits, the dayside IMB locations at different SZA were all extrapolated to the terminator altitude. We assumed that every position of the IMB expands with a same ratio: $\text{Alt}_{\text{ter}}/1258 = \text{Alt}/\text{Alt(SZA)}$, where the Alt(SZA) is defined by Eq. (1), and 1258 is the terminator altitude from Eq. (1). For each measured altitude Alt, an extrapolated altitude at the terminator can be given by Alt_{ter}. The stronger solar activity indicates stronger EUV irradiance, which has an effect on the ionopause (Han et al. 2020). In Fig. 3a, the solar activity-dependence is quantitatively evaluated roughly by the SSN for lacking local EUV measurements. The influence of solar activity is eliminated: the IMB altitude = $\text{Alt}_{\text{ter}} + 2.42 \times (\text{SSN} - 67)$.

Table 1. Average IMB locations at solar maximum and solar minimum.

	Solarmax	Solarmin	Solarmax
Period	12.1978–12.1980	04.2006–08.2006	07.2011–11.2014
Orbiter	PVO	VEX	VEX
Solar cycle	21	24	24
SSN	210	18	67
Subsolar altitude (km)	498	299	387
Terminator altitude (km)	1700	1013	1258
	Zhang et al. (1991)	Zhang et al. (2008a)	This study
Average solar wind (SW) and IMF conditions at 0.72 AU			
Period [(a)]	12.1978–12.1981	01.2008–12.2009	07.2011–11.2014
N_{SW} (cm^{-3})	17.0	6.9	4.5
V_{SW} ($km\,s^{-1}$)	400	376	372
IMF magnitude (nT) [(a)]	12.1	6.5	8.8
IMF cone angle (°) [(a)]	54	56	57

Notes. [(a)] Adopted from Chang et al. (2018).

The average solar wind density and velocity derived from ASPERA-4 are 4.5 cm^{-3} and 372 $km\,s^{-1}$, respectively, at solar maximum (July 2011–November 2014), while the average IMF magnitude and IMF cone angle are 8.8 nT and 57°, respectively (Chang et al. 2018). The solar wind dynamic pressure controls the IMB altitude significantly, as shown in Fig. 3b. This is consistent with the result from the PVO observation (Zhang et al. 1991). It has been demonstrated that the ionopause altitude decreases with the enhanced solar wind dynamic pressure (Elphic et al. 1980; Phillips et al. 1984; Russell et al. 2006; Angsmann et al. 2011). Since the ionopause is the lower boundary of the Venusian-induced magnetosphere, a lower ionopause suggests a lower IMB. In Figs. 3c and d, we carried out the regressions of the solar wind density and velocity. The IMB altitude shows no evident trend (P-Value > 0.01) with solar wind velocity (v_{sw}) though the increase in v_{sw} influences the solar wind dynamic pressure ($P_{dyn} = \rho v_{sw}^2$). We note that the median IMBs (green dots) under fast solar wind ($v_{sw} > 500\,km\,s^{-1}$) are anticorrelated to the solar wind speed. They might be related to high dynamic pressure structures, such as corotating interaction regions.

Figure 4 displays the variation of the IMB altitude on the IMF condition. To minimize the influence of solar wind dynamic pressure, the IMB altitude data were normalized to the average solar wind dynamic pressure according to Formisano (1979): $R_0 = R \times (P_{dyn}/P_{dyn0})^{1/6}$, where R_0 is the normalized IMB altitude, P_{dyn0} is the average dynamic pressure, R is the observed IMB altitude in the previous section, and P_{dyn} is the measured solar wind pressure. To avoid the space whether effect, we ignored the data in which $v_{sw} > 500\,km\,s^{-1}$. There is no obvious dependence (P-value > 0.01) of the IMB altitude on the total IMF magnitude, but a notable increase in the IMB altitude with the IMF cone angle ($\arccos(|B_X/B|)$) is observed from Fig. 4b. The result of linear regression suggests that the IMF orientation has control of the Venusian IMB location.

The decrease in the IMB altitude with the IMF cone angle can be explained by the influence of the IMF on the Venusian ionosphere. Chang et al. (2020) have reported that the external pressure applied on the ionosphere decreases when the IMF cone angle is small. Xiao & Zhang (2018) observed weaker magnetic pressure of the induced magnetosphere during small IMF cone angles (0°–30°) compared with those under the condition of large IMF cone angles (60°–90°). The ionosphere will expand when the outside pressure decreases (Russell et al. 2006). Consequently, the ionopause is higher for the small IMF cone angle and the whole induced magnetosphere is elevated. However, it should be mentioned that the induced magnetosphere will disappear when the cone angle is 0° or the IMF would be perfectly aligned with the solar wind flow (Zhang et al. 2009). Based on the appearance of photoelectrons and the sharp decrease in magnetic field strength (Bertucci et al. 2011), we picked out 435 clear ionopause crossings at solar maximum. The ionopause altitude changes little with SZA and EUV because the data points of VEX are concentrated at a high-SZA region, and the low EUV radiation in Solar Cycle 24 has a small effect (Han et al. 2020). We checked the dependence of the ionopause on SZA and daily SSN and found that the correlations are negligible. Figure 4c shows the decrease in ionopause altitude (normalized to average P_{dyn}) with an increasing IMF cone angle. We note that the slope of Fig. 4c is smoother in comparison with Fig. 4b. We think some other factors also play roles. In Fig. 4d, the peak value of the magnetic pressure in the induced magnetosphere is higher when the IMF cone angle increases. The IMF orientation has an effect on the strength of the induced magnetosphere. This result is consistent with Xiao & Zhang (2018).

4. Discussions and conclusions

The features of the IMB are determined by the massloading effect as well as the IMF conditions and they should be different from case to case. The massloaded magnetic field can be regarded as quasi-static or fossil. The induced magnetosphere can be treated as a part of Venus, in analogy to Earth's intrinsic magnetosphere. Therefore, when the IMF is quite different from the fixed magnetic field within the induced magnetosphere, an apparent magnetic rotation takes place at the IMB. When the IMF is close to the fixed magnetic field, such magnetic rotation could be very smooth. The variation in magnetic strength across the IMB can also be very different due to the thermal pressure gradient at the IMB. The magnetosheath plasma pressure has little contribution at the IMB if the magnetic field strength is strong in the inner magnetosheath. In this case, sheath protons

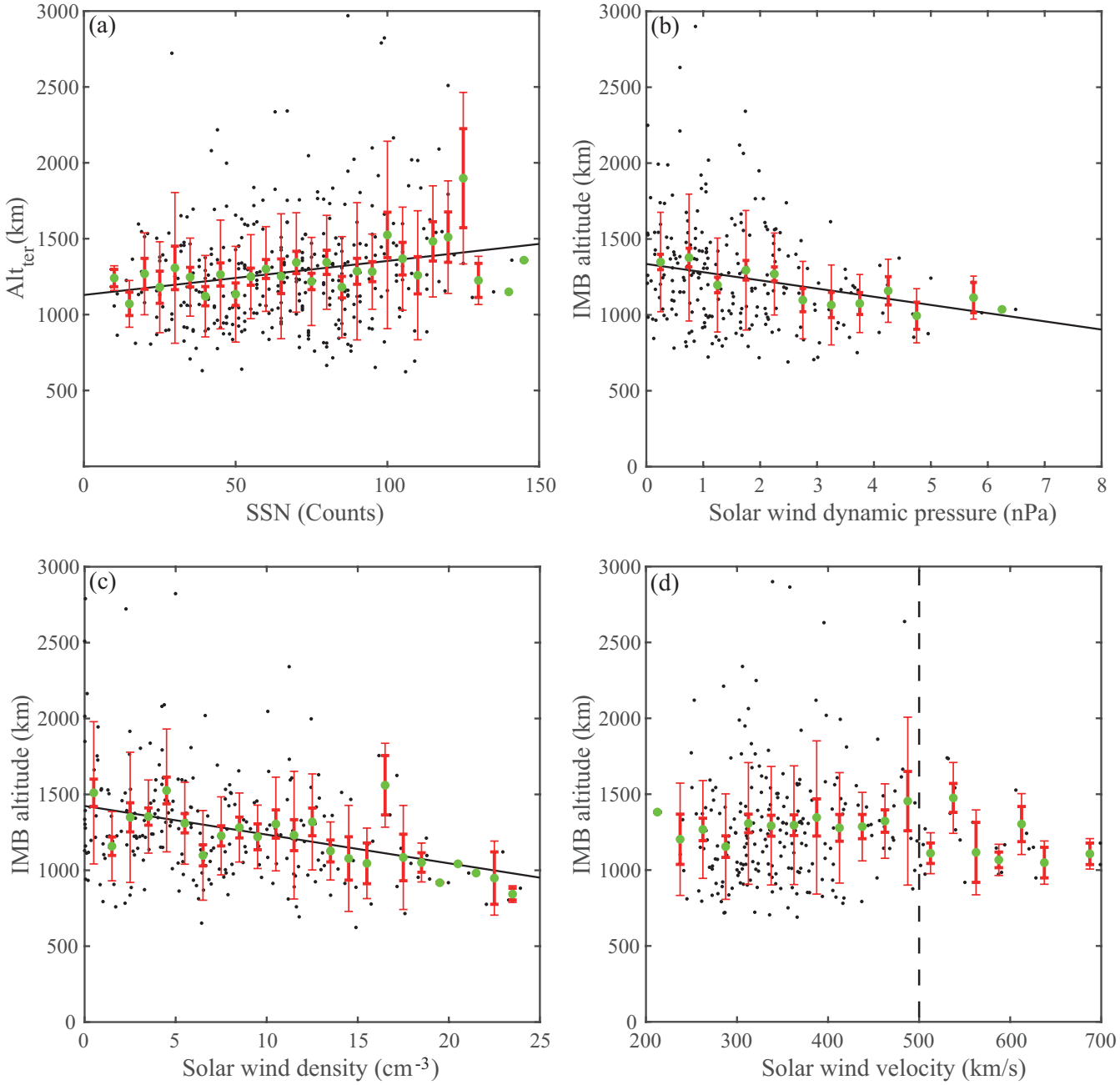

Fig. 3. Dependence of IMB altitude on the solar activity and on the solar wind parameters. (*a*) The extrapolated terminator IMB altitudes Alt_{ter} (black points) distribute with the sunspot number (SSN) observed from the Earth. A linear regression (black line) was done to all of the data points. The mean Alt_{ter} in SSN bins of 5 Counts (green dots), the standard deviation in each bin (thin red error bars), and the standard error of the mean (thick red error bars) are shown. (*b–d*) Similar to (a), but the Alt_{ter} was normalized to the average SSN and is referred as the "IMB altitude." There is no correlation between the IMB altitude and the solar wind velocity (*P*-value > 0.01).

are depleted gradually by the strong magnetic field before arriving at the IMB and the magnetic magnitude variation across the IMB could be gradual.

The well-structured Venusian-induced magnetosphere boundary is investigated in this study. Similar to the Earth's magnetopause, the Venusian IMB defines two regimes upstream and downstream of the boundary. From the VEX's observation, the IMB can be well determined based on the changes in the magnetic field and plasma flux. The IMB consists of a discontinuity (Zhang et al. 2008b) separating the planetary cold ions from the hot magnetosheath protons. The depletion of the shocked solar wind plasma at the IMB suggests that the scale of the IMB represents the size of the planet obstacle. Zhang et al. (2007) calculated the Venus bow shock position based on the measurements of the IMB position (the real obstacle) and found that the calculated result is coincident with the observed bow shock position. We statistically analyzed the average IMB position at solar maximum of Solar Cycle 24. Jointly with previous observations, the position of the IMB is dependent on solar activities. The IMB moves to higher altitudes as the solar activity is stronger. In addition, the solar wind and IMF have control on the IMB position. The IMB altitude decreases with increasing solar wind dynamic pressure and an increasing IMF cone angle, while the IMB location is independent of the

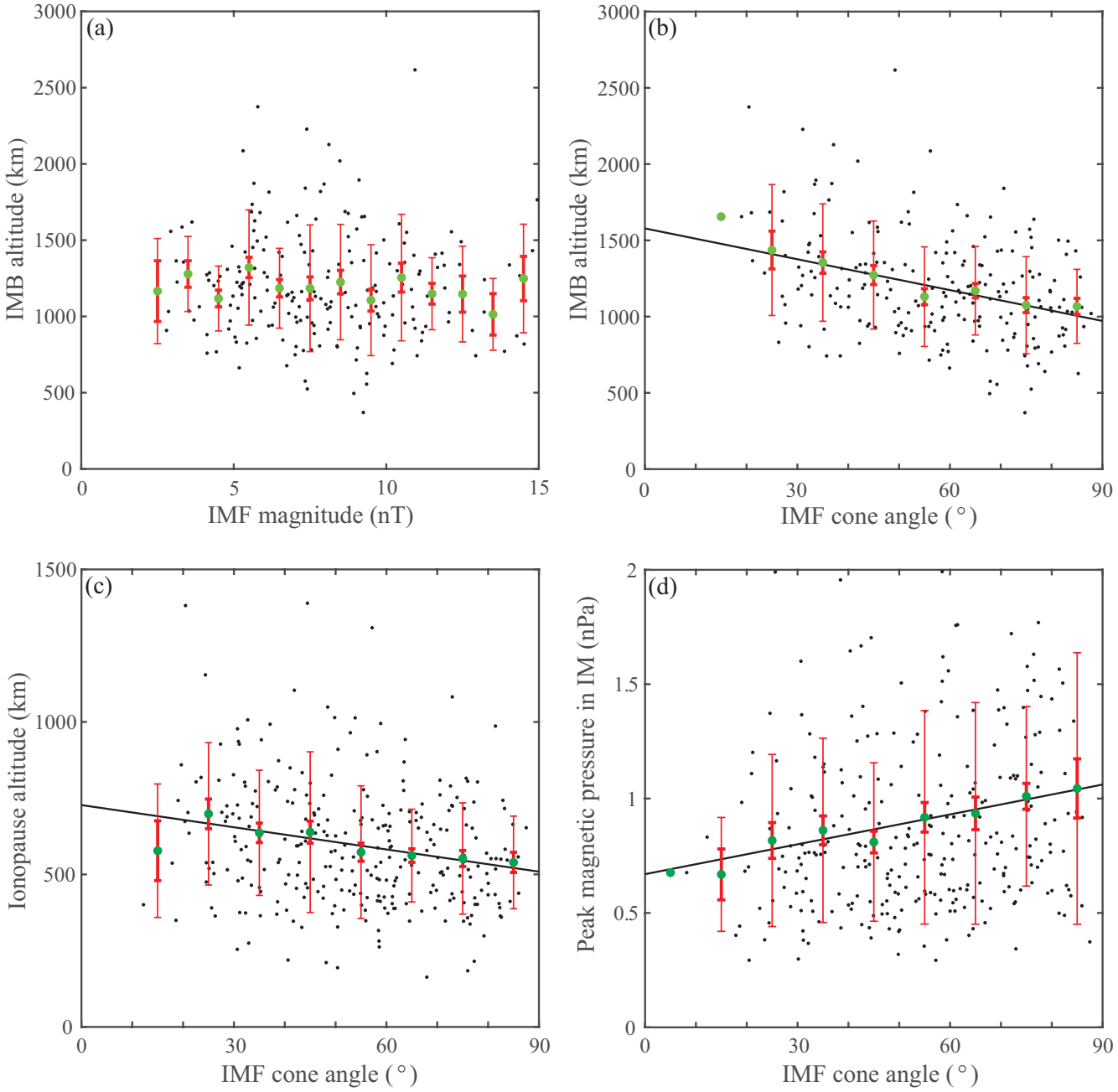

Fig. 4. Dependence of Venusian IMB and ionopause altitude on the IMF. (*a–b*) Similar to Fig. 3, but the terminator IMB altitude is further normalized to the average SSN and average solar wind dynamic pressure. (*c*) The control of the IMF cone angle on the Venusian ionopause altitude normalized to the average solar wind dynamic pressure. (*d*) The control of the IMF cone angle on the peak value of the magnetic pressure in the induced magnetosphere (IM). Linear regressions (black line) were done to all of the data points (black points). The mean IMB altitude, the mean ionopause altitude and THE mean magnetic pressure in bins (green dots), the standard deviation in each bin (thin red error bars), and the standard error of the mean (thick red error bars) are shown. There is no correlation between the IMB altitude and the IMF magnitude (P-value > 0.01).

IMF magnitude. Since the solar wind velocity contributes to the dynamic pressure ($P_{\rm dyn} = \rho v_{\rm sw}^2$), the increase in $v_{\rm sw}$ should have an influence on the IMB. However, our regression results indicate that there is no dependence of the IMB location on $v_{\rm sw}$. We propose a possible explanation that the solar wind velocity has an effect on the pileup of the IMF above the ionopause, which leads to a thicker induced magnetosphere. Even though the increased dynamic pressure would compress the ionosphere, the IMB position will not vary significantly with the solar wind velocity for the compensation from a thicker induced magnetosphere. However, the thickness of the Venusian-induced magnetosphere was not discussed as much before and more effort needs to be put in. The dependence of the IMB location on the IMF is attributed to the variation in the ionopause since the ionopause location can strongly affect the IMB location. The pressure of the induced magnetosphere is stronger under a large IMF cone angle and the ionosphere is compressed consequently. In this way, the altitudes of the ionopause and IMB decrease.

Acknowledgements. The authors acknowledge Venus Express team for providing the magnetic field data and plasma data at ESA's Planetary Science Archive (ftp://psa.esac.esa.int/pub/mirror/VENUS-EXPRESS/). The

solar wind moment data are available at AMDA (http://amda.cdpp.eu/) science analysis system provided by the Centre de Données de la Physique des Plasmas (CDPP) supported by CNRS, CNES, Observatoire de Paris and Université Paul Sabatier, Toulouse. We also thank the World Data Center SILSO (http://www.sidc.be/silso/) for using the sunspot number data. This work is funded by The Science and Technology Development Fund, Macau SAR (File no. 0002/2019/A1), Macau Foundation, the pre-research project on Civil Aerospace Technologies No. D020308 and D020104 funded by China National Space Administration, supported by international partnership program of Chinese Academy of Sciences under grant no. 183311KYSB20200017.

References

Angsmann, A., Fränz, M., Dubinin, E., et al. 2011, Planet. Space Sci., 59, 327
Barabash, S., Sauvaud, J. A., Gunell, H., et al. 2007a, Planet. Space Sci., 55, 1772
Barabash, S., Fedorov, A., Sauvaud, J. J., et al. 2007b, Nature, 450, 650
Bertucci, C., Mazelle, C., Slavin, J. A., et al. 2003, Geophys. Res. Lett., 30, 1876
Bertucci, C., Mazelle, C., Acuna, M. H., et al. 2005, J. Geophys. Res. (Space Phys.), 110, 1209
Bertucci, C., Duru, F., Edberg, N., et al. 2011, Space Sci. Rev., 162, 113
Chai, L., Fraenz, M., Wan, W., et al. 2014, J. Geophys. Res. (Space Phys.), 119, 9464
Chang, Q., Xu, X., Zhang, T., et al. 2018, ApJ, 867, 129
Chang, Q., Xu, X., Xu, Q., et al. 2020, ApJ, 900, 9
Coates, A. J., Frahm, R. A., Linder, D. R., et al. 2008, Planet. Space Sci., 56, 802
Collinson, G. A., Grebowsky, J., Sibeck, D. G., et al. 2015, J. Geophys. Res. (Space Phys.), 120, 3489
Cui, J., Galand, M., Coates, A. J., et al. 2011, J. Geophys. Res. (Space Phys.), 116, A04321
Dubinin, E. M., Sauer, K., & McKenzie, J. F. 2006, Annales Geophysicae, 24, 3041
Dubinin, E., Fraenz, M., Fedorov, A., et al. 2011, Space Sci. Rev., 162, 173
Elphic, R. C., Russell, C. T., Slavin, J. A., et al. 1980, J. Geophys. Res. (Space Phys.), 85, 7679
Fedorov, A., Ferrier, C., Sauvaud, J. A., et al. 2008, Planet. Space Sci., 56, 812
Fedorov, A., Barabash, S., Sauvaud, J. A., et al. 2011, J. Geophys. Res. (Space Phys.), 116, 7220
Formisano, V. 1979, Planet. Space Sci., 27, 1151
Fox, J. L., & Sung, K. Y. 2001, J. Geophys. Res. (Space Phys.), 106, 21305
Han, Q., Fraenz, M., Wei, Y., et al. 2020, Earth Planet. Phys., 4, 73
Luhmann, J. G., Ledvina, S. A., & Russell, C. T. 2004, Adv. Space Res., 33, 1905
Ma, Y., Toth, G., Nagy, A., et al. 2020, Geophys. Res. Lett., 47, e87593
Martinecz, C., Fränz, M., Woch, J., et al. 2008, Planet. Space Sci., 56, 780
Martinecz, C., Boesswetter, A., Fränz, M., et al. 2009, J. Geophys. Res. (Planets), 114, E00B30
Øieroset, M., Mitchell, D. L., Phan, T. D., et al. 2004, Space Sci. Rev., 111, 185
Phillips, J. L., & McComas, D. J. 1991, Space Sci. Rev., 55, 1
Phillips, J. L., Luhmann, J. G., & Russell, C. T. 1984, J. Geophys. Res. (Space Phys.), 89, 10676
Rong, Z. J., Barabash, S., Futaana, Y., et al. 2014, J. Geophys. Res. (Space Phys.), 119, 8838
Russell, C. T., Chou, E., Luhmann, J. G., et al. 1988, J. Geophys. Res. (Space Phys.), 93, 5461
Russell, C. T., Luhmann, J. G., & Strangeway, R. J. 2006, Planet. Space Sci., 54, 1482
Saunders, M. A., & Russell, C. T. 1986, J. Geophys. Res. (Space Phys.), 91, 5589
Spenner, K., Knudsen, W. C., Miller, K. L., et al. 1980, J. Geophys. Res. (Space Phys.), 85, 7655
Svedhem, H., Titov, D. V., McCoy, D., et al. 2007, Planet. Space Sci., 55, 1636
Vaisberg, O. L., Romanov, S. A., Smirnov, V. N., et al. 1976, Phys. Solar Planet. Environ., 8, 904
Wang, J., Lee, L. C., Xu, X., et al. 2020, A&A, 642, 34
Xiao, S. D., & Zhang, T. L. 2018, Planet. Space Sci., 158, 53
Xu, Q., Xu, X., Chang, Q., et al. 2019, ApJ, 876, 84
Zhang, T. L., Luhmann, J. G., & Russell, C. T. 1990, J. Geophys. Res. (Space Phys.), 95, 14961
Zhang, T. L., Luhmann, J. G., & Russell, C. T. 1991, J. Geophys. Res. (Space Phys.), 96, 11145
Zhang, T. L., Baumjohann, W., Delva, M., et al. 2006, Planet. Space Sci., 54, 1336
Zhang, T. L., Delva, M., Baumjohann, W., et al. 2007, Nature, 450, 654
Zhang, T. L., Delva, M., Baumjohann, W., et al. 2008a, Planet. Space Sci., 56, 790
Zhang, T. L., Delva, M., Baumjohann, W., et al. 2008b, J. Geophys. Res. (Planets), 113, E00B20
Zhang, T. L., Du, J., Ma, Y. J., et al. 2009, Geophys. Res. Lett., 36, L20203